This is a repository copy of *Application of grinding to reduce rail side wear in straight track*.

White Rose Research Online URL for this paper:
http://eprints.whiterose.ac.uk/128105/

Version: Accepted Version

Article:
Ding, J., Lewis, R., Beagles, A. orcid.org/0000-0001-8306-5632 et al. (1 more author) (2018) Application of grinding to reduce rail side wear in straight track. Wear, 402-40. pp. 71-79. ISSN 0043-1648

https://doi.org/10.1016/j.wear.2018.02.001

Reuse
Items deposited in White Rose Research Online are protected by copyright, with all rights reserved unless indicated otherwise. They may be downloaded and/or printed for private study, or other acts as permitted by national copyright laws. The publisher or other rights holders may allow further reproduction and re-use of the full text version. This is indicated by the licence information on the White Rose Research Online record for the item.

Takedown
If you consider content in White Rose Research Online to be in breach of UK law, please notify us by emailing eprints@whiterose.ac.uk including the URL of the record and the reason for the withdrawal request.

eprints@whiterose.ac.uk
https://eprints.whiterose.ac.uk/

Application of Grinding to Reduce Rail Side Wear in Straight track

Junjun Ding [a], Roger Lewis [b], Adam Beagles [b], Junping Wang [c]

[a] School of Mechanics Engineering, Southwest Jiaotong University, Chengdu 610031, Sichuan, China

[b] Department of Mechanical Engineering, The University of Sheffield, Mappin Street,S13JDUK

[c] China Railway Materials Track Technology Service Group Co. Ltd. Beijing 100036, China

ABSTRACT： A stretch of straight rail on the Jing-Hu railway in China has been suffering from unacceptable levels of side wear. This phenomenon has not previously been investigated. This paper reports on work to analyse the causes using actual wheel and rail profiles from the track where it has occurred and a novel contact assessment approach and possible mitigations. By running a range of dynamic multibody simulations, it was shown that static calculations are adequate to represent the contact conditions that cause the wear. Almost 7000 wheel profiles were measured and their contact with the relevant rail profile calculated. It was predicted that freight trains whose wheels have a large rolling radius difference, would rub on the gauge corner and gauge face, thus causing the wear. This finding was consistent with field measurements.

Two grinding strategies were developed that could reduce the number of damaging contacts. These were, grinding the gauge shoulder, and grinding the field side of the top of the rail. Calculations predicted that the largest improvement would result from combining both strategies. This approach was adopted to reduce the side wear on rail in straight track. It was found that the distribution of wheel/rail contact points on the rail surface agreed well with the calculation results, and the proposed grinding regime did reduce side wear.

Key words： wheel/rail profile; side wear; rail grinding; rolling radius difference

1 Introduction

Wheel/rail wear is a normal phenomenon, and becomes more serious as vehicles' running speed and axle load increase. In most railways, wheel and rail life are limited by wheel flange wear and rail side wear. In order to reduce wheel/rail wear, many studies have been performed worldwide.

Managing the contact conditions between wheel and rail is key to controlling rail defect initiation and growth [1], and the major influences on wheel and rail wear can only be understood by analysing the contact between them. A number of different applications of contact mechanics to reduce damage problems have been reported. In order to improve rolling contact fatigue and wear performance, Magel et al. applied a quasi-static curving analysis combined with Hertzian normal contact and a linear wheel/rail lateral contact model to optimize wheel and rail profiles [2, 3]. Choi et al. employed a genetic-algorithm-based optimization method to design an asymmetric rail head profile that can reduce rail wear (predicted by post-processing results from commercial software) on curved tracks [4]. Shevtsov et al. [5] used static geometric contact analyses to design a wheel profile; they used an optimality criterion based on a rolling radius difference (RRD) function, but ran commercial software to verify that the profiles satisfied stability, wear, and dynamic contact stress requirements. Zhai et al. developed a design methodology for asymmetrically ground rail profiles to reduce side wear on heavy-haul railway curves [6]. Their contact calculations used Hertzian theory and with lateral forces given by a nonlinear heuristic model. No studies though have used actual profiles as an input and assessed the impact of proposed changes through track trials.

There has been significant progress in the simulation of wheel/rail wear evolution in recent years. Braghin developed a fast and reliable mathematical model to predict wheel profile evolution caused by

wear [7]. He used multi-Hertzian calculations for the normal forces and a heuristic tangential contact force model. In order to simulate the wear evaluation of wheel profiles more accurately, Enblom considered the impact of materials' elastic shear deformation on slip velocity to produce an improvement to Kalker's Fastsim and considered the influence of disk braking and lubrication conditions on wheel wear [8]. Lewis et al. produced maps of rail material wear coefficients taken from laboratory tests run on twin disc and pin-on-disc machines [9]. Ignesti and Innocenti used a novel procedure to speed-up the calculation of initial contact and presented an accurate wear model to predict wheel and rail profile evolution due to wear specifically for complex railway networks [10, 11]. Other wheel/rail material wear models have been built based on dissipated energy, the flow density of energy dissipated, and the Archard wear modelling approach [12, 13, 14]. Enblom [8], Jin et al. [15], and Li et al. [16], amongst others, predicted the evolution of rail wear by combining vehicle dynamical models and wear maps.

Some researchers have focused on the parameters of track and vehicle. By numerical simulation, Adachi et al. concluded that gauge widening, and having a larger inclination angle for the inner rail, are both effective for reducing rail wear [17]. Povilaitienė et al. investigated the influence of gauge widening on rail side wear in curves. The results indicated that track widening to decrease wear can be of vital importance [18]. Ji et al. concluded that curve radius and running speed are the critical factors affecting rail side wear [19]. Cui et al. investigated the effect of primary yaw stiffness on rail side wear in curves, and proposed a parallel inverse method to design a new wheel profile for reducing rail side wear [20]. Other techniques such as rail lubrication [21, 22] and top-of-rail (TOR) friction control [23, 24] are also applied to reduce rail wear. For straight track, it has not been established that gauge widening reduces side wear. To protect large distances of straight track, the installation and maintenance of a rail lubrication system would be prohibitively expensive and impractical. Abnormal rail wear always results from bad wheel/rail contact geometry, so rail grinding is used to reduce rail wear, with most grinding work focused on curved track.

In straight track, most rail wear is located at the TOR, and the wear rate is much less than that in curved track. For rail in straight track, most researchers focus on rolling contact fatigue (RCF) [25] and hunting (lateral oscillation of a vehicle) instability [26, 27]. However, in recent years, there have been more reports of side wear occurring on straight track. Example rail surfaces are shown in Fig.1. There are two wear zones on the rail surface, one is on the TOR and the other is on the rail gauge corner and gauge face. Side wear in straight track progresses more slowly than in curved track, but the resulting abnormal wheel/rail contacts will affect the dynamic performance of vehicles and could lead to hunting instability if the wear produced a high equivalent conicity. The maintenance engineers responsible for the rail shown in Fig.1 were concerned about safety and other implications of the side wear. They wanted to know if hunting was responsible for it appearing, and how to avoid this abnormal phenomenon.

Problems associated with rail side wear in straight track have not received much attention, with almost no published research on this phenomenon. In order to avoid or reduce side wear in straight track, it is important to analyse the causes of this phenomenon. Based on a large number of measured wheel profiles, this paper analyses the causes of side wear in straight track, using wheel/rail contact point distributions. The influences of passenger and freight vehicles on rail side wear are also considered. Having identified the causes of side wear in straight track, this paper reports on the development and implementation of a grinding strategy that reduces it.

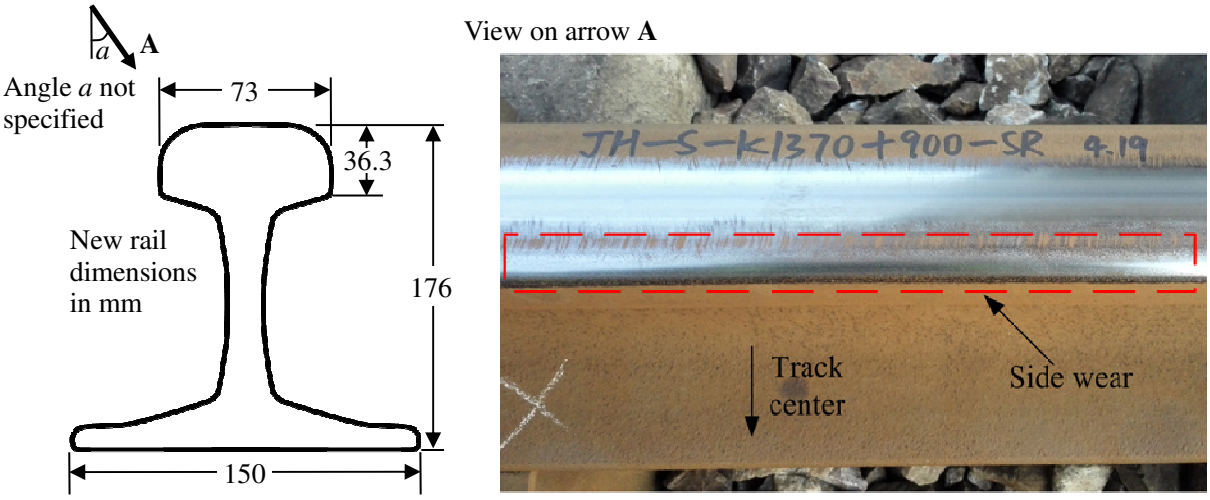

Fig.1. Rail surfaces with side wear in straight track

2 Wheel/rail profile measurements

2.1 Rail profile measurements

The rail surface shown in Fig.1 comes from the Jing-Hu railway located in the east of China. The number 1370 written on the rail indicates the mileage along the route. In this paper, Rail:1370 indicates the rail at a distance of 1370 km along this track. The calculations and field trials were carried out for rail at this location.

The profiles of Rail:1370 were measured using a MiniProf machine. The left and right rail of Rail:1370 have similar profiles, so only the right rail profile was used in this paper. Both the measured rail profile (thin line) and new rail profile (bold line) are shown in Fig.2. The new rail profile on the Jing-Hu railway is CN60 with a weight per metre of 60 kg. Rail profiles can be divided into different zones according to the wheel/rail contact position. Side wear is considered to occur if the angle between the normal to the rail profile at the wear position and the rail centreline is larger than 15° (near the boundary between the R13 arc and R80 arc, as shown in Fig.2).

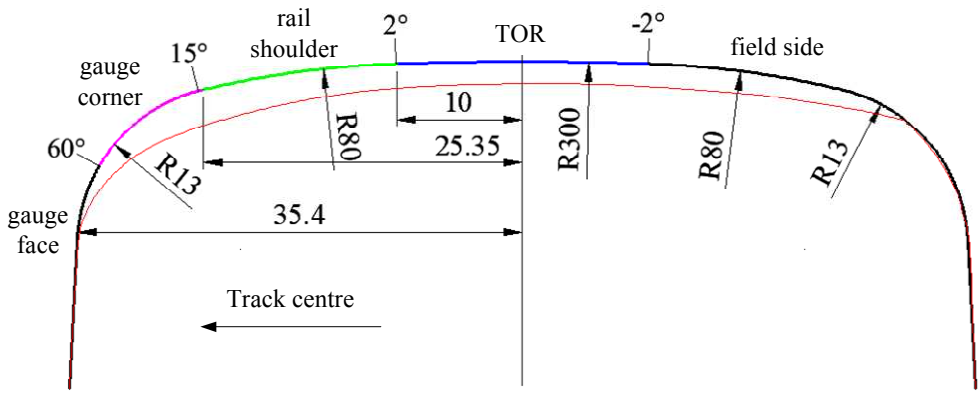

Fig.2. Rail:1370 and new rail profiles showing radii, angles, and definitions of zones of CN60 rail (TOR is "Top of Rail")

The rail steel material of Jing-Hu railway is U75V. The chemical composition of U75V steel is listed in Table 1. The tensile strength of this kind of U75V rail steel is ≥980MPa. Meanwhile, the hardness value is 270-300 HB.

Table 1: Chemical composition of U75V rail steel

Composition	C	Si	Mn	P	S	V	Nb
Content/%	0.71-0.80	0.50-0.80	0.70-1.05	≤0.030	≤0.030	0.04-0.12	≤0.010

2.2 Wheel profile measurement

The annual traffic volume over Rail:1370 is about 100 MGt, with about 45 freight trains and 73 passenger trains passing every day.

In order to predict the full range of wheel/rail contact conditions, a large number of wheel profiles from passenger vehicles and freight wagons that run on the Jing-Hu railway were measured. The number of wheel profiles from passenger vehicles was 956 (from 478 wheelsets), and from freight wagons was 5876 (from 2938 wheelsets). Fig.3 shows a superposition of all of the measured wheel profiles to enable their range to be visualised.

There is often a difference in the radius of the left and right wheel in the same wheelset. This could result from a manufacturing error, from asymmetric wear in service, or from different grinding depths being required to remove defects at overhaul. So, the radii of the wheels were measured along with the wheel profiles. The Nominal Running Radius Difference (NRRD) data was calculated for both passenger and freight vehicles. The distributions of the NRRD are shown in Table 2, Table 3, and Fig 4.

In Chinese railways, passenger vehicles are always well maintained to ensure good ride comfort, so the bogies and wheelsets are maintained frequently. Most of the NRRD of passenger vehicles' wheels were less than 0.5 mm and the maximum NRRD did not exceed 2.5 mm. For freight vehicles, because of the higher axle load, larger acceptable tolerances, and longer maintenance periodicities, the NRRDs are larger than for passenger vehicles; their maximum NRRD is 8 mm.

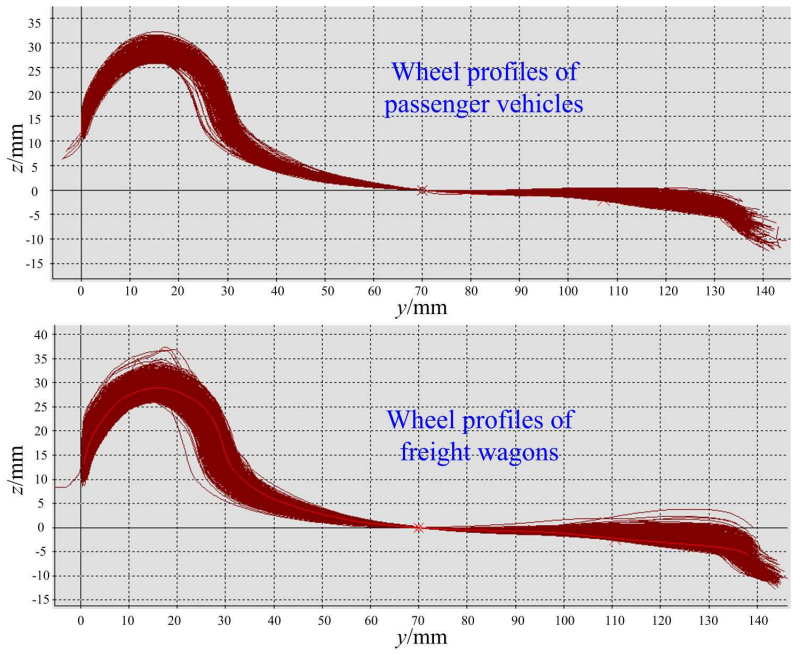

Fig.3. Measured wheel profiles, where y is the distance from the wheel's datum face, and z the radius difference from the gauge point (70 mm outboard of datum)

Table 2: NRRD distribution for passenger vehicles

NRRD range/mm	0 - 0.5	0.5 - 1	1.0 - 1.5	1.5 - 2.0	2.0 - 2.5
Number of wheelsets	360	85	22	8	3
Proportion/%	75.3	17.8	4.6	1.7	0.6

Table 3: NRRD distribution for freight vehicles

NRRD range/mm	0 - 1	1 - 2	2 - 3	3 - 4	4 - 5	≥ 5
Number of wheelsets	2344	364	131	62	22	15
Proportion/%	79.8	12.4	4.5	2.1	0.7	0.5

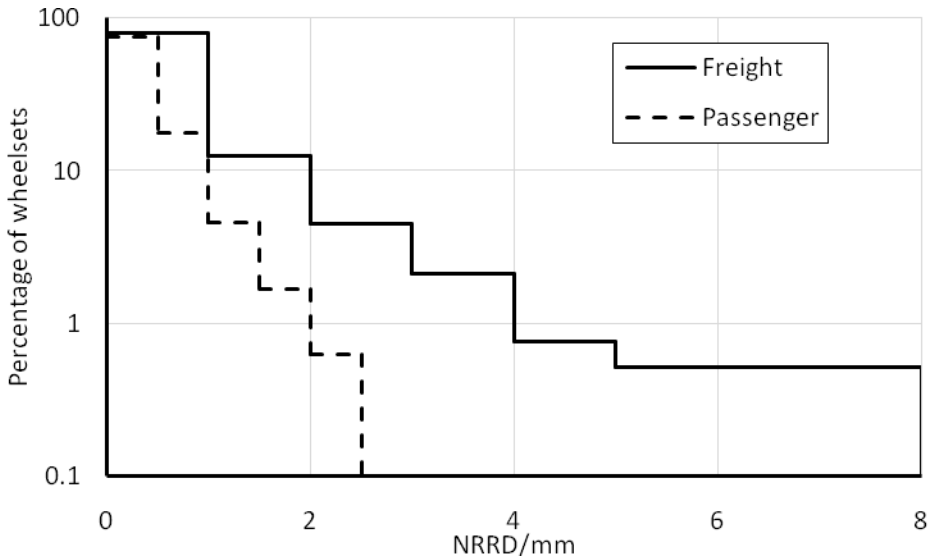

Fig.4. Comparison of NRRD distributions of freight and passenger vehicles

3 Vehicle dynamic simulations

3.1 Vehicle dynamic models

In order to analyse the vehicles' dynamic behaviour when passing over Rail:1370, dynamic models of appropriate passenger and freight vehicles were built in SIMPACK MBS dynamic software [28]. For the simulations, the wheel/rail contact model considered multipoint contact. Hertzian contact theory and Kalker's simplified theory FASTSIM [29] were used to calculate the contact patch size and creep force; the friction coefficient was 0.4. Appropriate track lateral irregularities (to drive any hunting accelerations) had amplitudes of about 8 mm, and wavelengths between 0.5 and 50 m. The flexibility of the track was not considered.

The passenger vehicle type is 25T with a SW-220K bogie. The freight vehicle type is C70 with a ZK6 bogie. The maximum running speed on the Jing-Hu railway for passenger and freight vehicles is 160 and 80 km/h respectively. The new wheel profile of both passenger and freight vehicle is type LM. The nominal rolling radius of a passenger vehicle's new wheel is 457.5 mm, and freight vehicle's is 420 mm.

Besides the new wheel profiles, 6 worn wheelsets (12 wheel profiles) with different NRRD as inputs to the dynamic models were selected. These wheelsets represented the range of NRRD and common features of wheels on the vehicles. These profiles are shown in Fig.5 and Fig.6. The wheel profiles from passenger vehicles have nearly no flange wear. For the freight vehicles, there are larger differences between the left and right wheel profile, and serious asymmetric wear and flange wear.

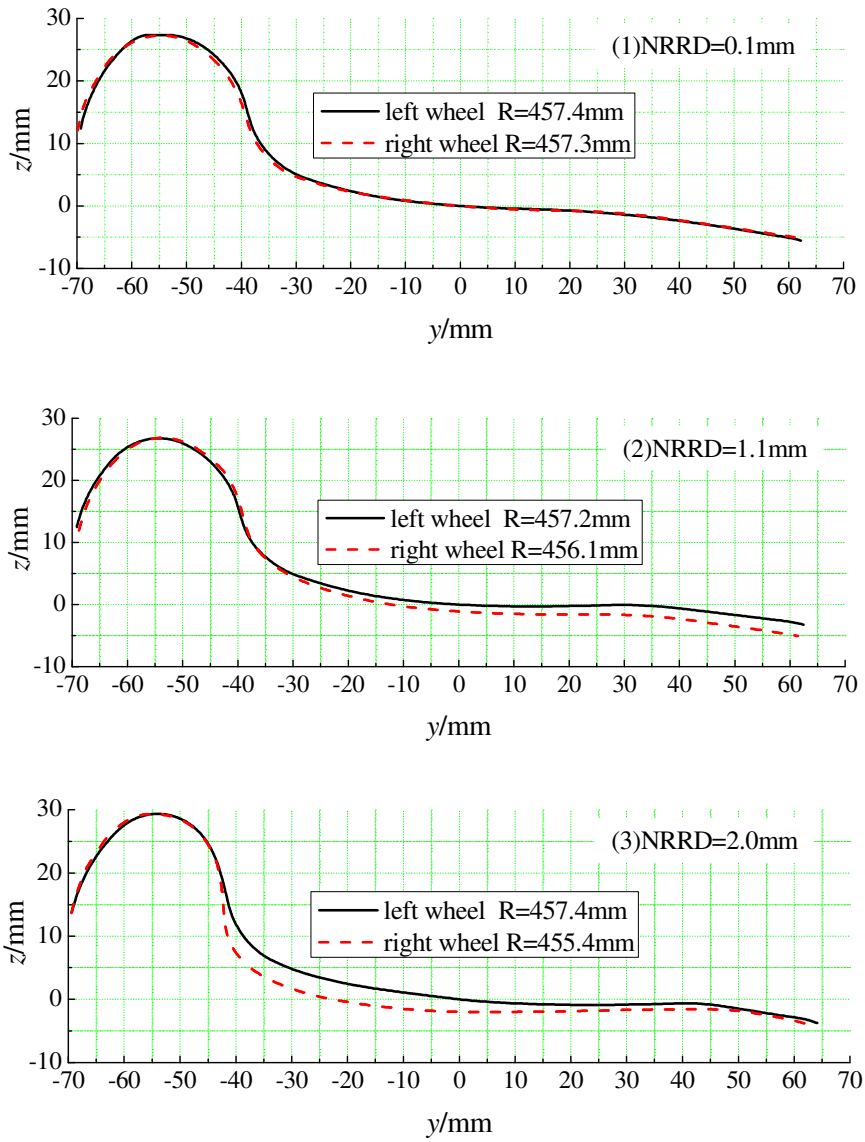

Fig.5. Worn wheel profiles of passenger vehicles

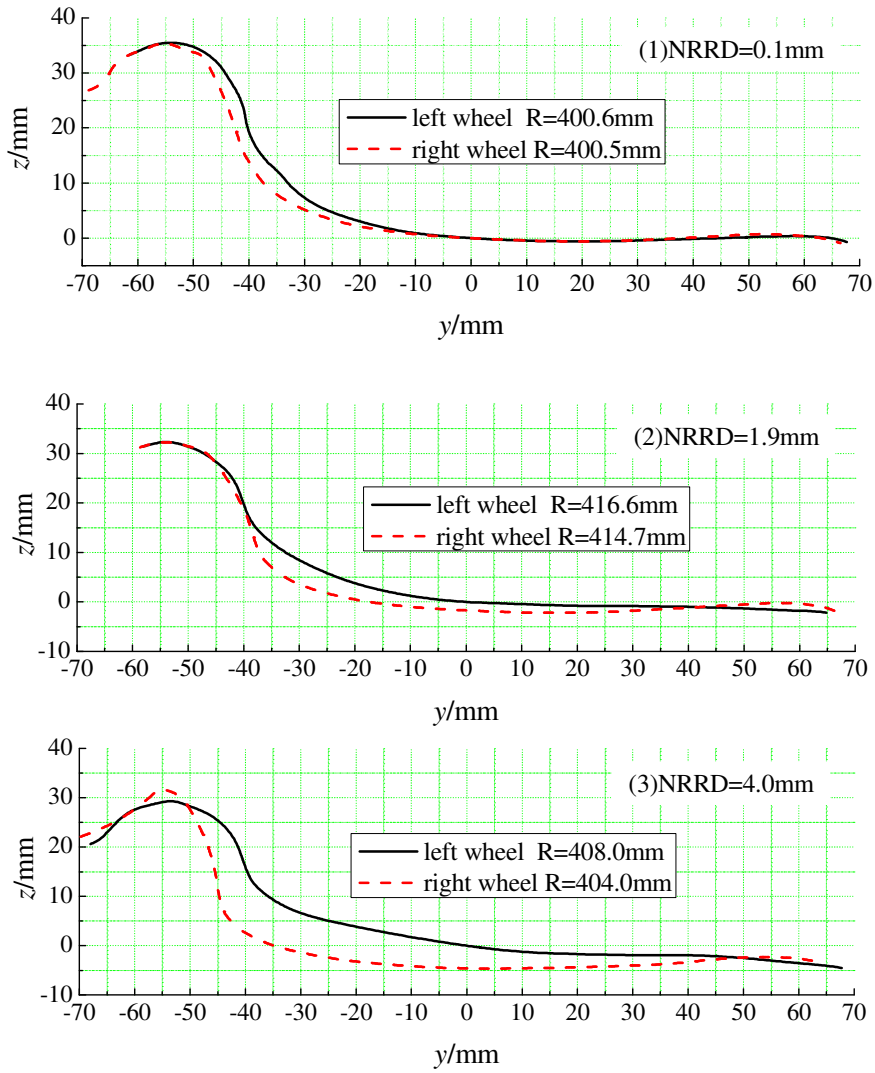

Fig.6. Worn wheel profiles of freight vehicles

3.2 Simulation results

For vehicles running on straight track, hunting instability was thought to be the most likely reason for rail side wear. Of the many methods to assess vehicle's hunting stability, the vehicle body lateral accelerations were used in this paper. Hunting was defined to occur when the standard deviation of the acceleration of the centre of the carbody, calculated from running over 600 m of track, exceeded 0.13 g [26].

When wheelsets run on straight track, the different radii of the wheels will result in them experiencing opposite direction longitudinal creep forces ($F_{x\mathrm{L}}$ and $F_{x\mathrm{R}}$. in Fig.7). These will cause a yaw rotation of the wheelset, its magnitude depending on the vehicle's primary suspension, and hence a non-zero angle of attack (AOA) φ_{w}, as shown in Fig.7. For equilibrium, to balance the torque from the longitudinal creep forces, the wheelset will experience lateral creep forces ($F_{y\mathrm{L}}$ and $F_{y\mathrm{R}}$). The AOA leads to it displacing laterally a distance y_{w}. In this balance position, the left and right wheels still have a small rolling radius difference to generate the creep forces that balance the creep forces associated with the AOA. Track irregularities will cause the wheelset to oscillate about the balance position, as shown in Fig.8.

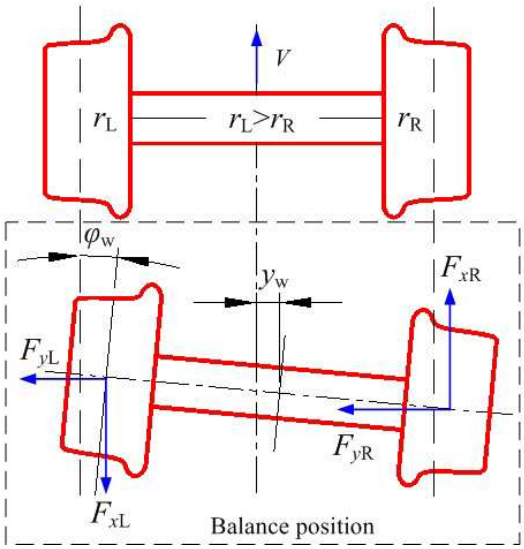

Fig.7. Balance position of wheelset

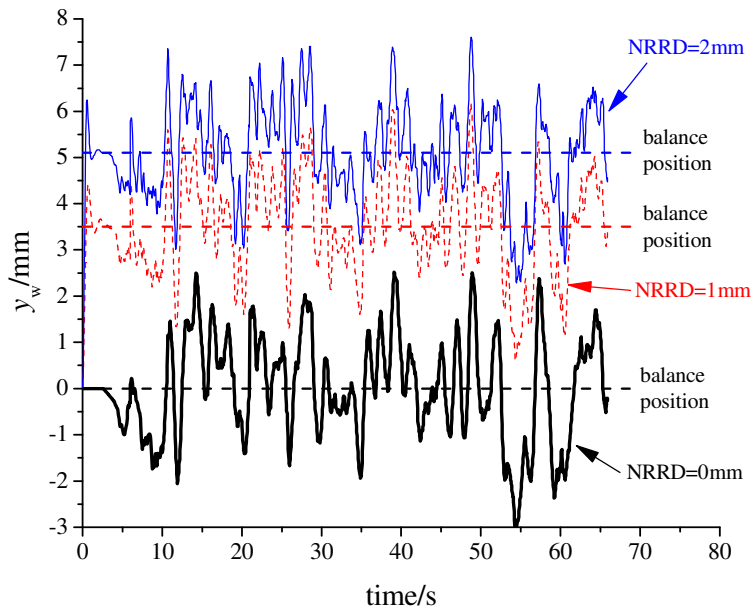

Fig.8. Lateral displacement of wheelsets with different NRRD

For passenger and freight vehicles running on straight track with the wheel profiles shown in Fig.7 and Fig.8, the effects of NRRD (the difference in the radii of the wheels at the gauge point) on the standard deviation of lateral carbody acceleration and on the wheelset balance positions are shown in Table 4 and Table 5. Note that, in these tables, the rolling radius difference (RRD) at balance point is the difference between the radii of the wheels at the contact points on each rail when in dynamic equilibrium.

Table 4: Dynamic simulation results for passenger vehicles

NRRD/mm	Standard deviation of lateral carbody acceleration/g		Balance position		
	half speed (80km/h)	top speed (160km/h)	y_w/mm	AOA/mrad	RRD /mm
0 (new wheel)	0.0106	0.0238	0	0	0
0.1	0.0109	0.0235	0.715	0.014	0.012
1.1	00142	0.0239	7.880	0.146	0.107
2.0	0.0282	0.0352	13.417	1.455	0.134

Table 5: Dynamic simulation results for freight vehicles

NRRD/mm	Standard deviation of lateral carbody acceleration/g		Balance position		
	half speed (40km/h)	top speed (80km/h)	y_w/mm	AOA/mrad	RRD /mm
0 (new wheel)	0.0149	0.0351	0	0	0
0.1	0.0156	0.0355	0.16	0.023	0.031
1.9	0.0289	0.0653	9.30	0.317	0.599
4.0	0.0302	0.0695	16.32	2.800	0.575

For passenger vehicles, when the running speed is 80km/h or 160 km/h, the standard deviation of lateral carbody acceleration will increase with RRD, but all the standard deviations for the different wheel profiles are less than 0.13 g. The freight vehicle at 40 km/h and 80 km/h has similar results to the passenger vehicle. No hunting instability has been predicted for either passenger or freight vehicles at Rail:1370. This is consistent with there having been no operational reports of hunting instability at this position on the Jing-Hu railway.

For wheelsets in the balance position, the lateral displacements increase rapidly with the NRRD, even more than they do with gauge widening. As can be seen in Tables 4 and 5, the RRD of the balance position is much less than the NRRD. This means that the NRRD is the key factor that affects wheelsets' lateral displacement. For subsequent contact calculations, the lateral displacements were calculated to give a zero RRD between the two wheels.

3.3 Discussion

The simulation results reported in Section 3.2 have shown that vehicles with a range of NRRD are predicted not to hunt. This stable running suggests that full dynamic simulations are not needed to determine the approximate locations and relative amounts of wear associated with running on the considered straight track. Accordingly, static geometric wheel/rail contact calculations were used to process the large number of combinations of profiles and NRRD required to investigate and mitigate the side wear phenomenon. Without this simplification, the computational effort would have been infeasible. To predict the magnitude of wear more accurately, contact conditions produced by dynamic calculations would need to be processed.

The results also show that the AOA associated with running at the lateral balance position only causes a very small RRD. This suggests that using a zero AOA, resulting in a zero RRD, will not have a significant effect on the results, so these conditions were implemented.

4. Effect of NRRD on rail contact positions

4.1 Contact point distribution on rail surface

The balance positions of wheelsets were determined by finding the zero of the RRD function (calculated using radii given by adding the relevant NRRDs to the profiles shown in Fig.3), a standard static geometric contact calculation. Each combination of wheel/rail profile contributed one or two contact points to the distribution on the rail profiles.

The geometric contacts between the measured wheel profiles and the rail profiles at Rail:1370 were analysed. The results are shown in Fig.9. Wheel/rail flange contact can only occur on the wheel with lower nominal rolling radius, so only the points of contact with this wheel are shown. The heights of the columns on the rail profile represent the number of contact points located in the corresponding area. Contact points on the gauge face and gauge corner (the side wear area) will lead to side wear, while others will not. Since the number of contact points is so large in some areas, the height scale is logarithmic.

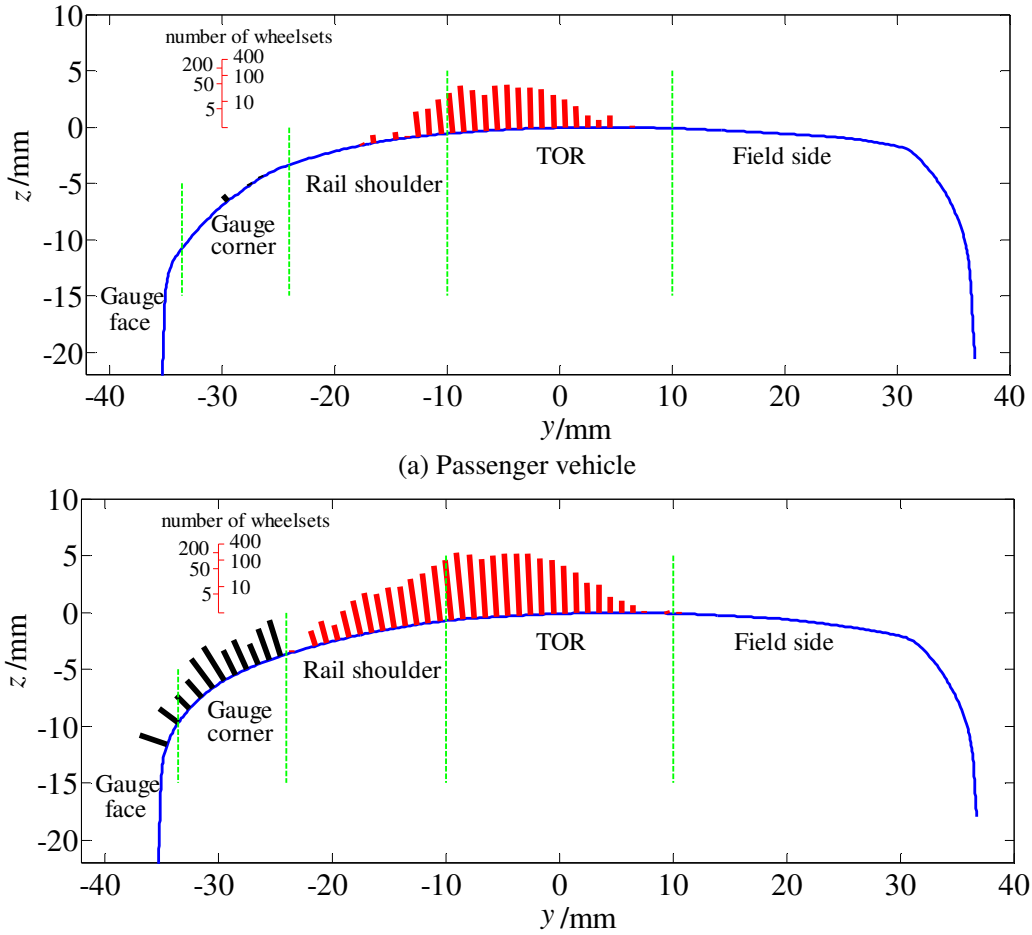

(a) Passenger vehicle

(b) Freight vehicle

Fig.9. Distributions of contact points on Rail:1370 profile, y and z are lateral and vertical distances respectively from TOR

Of the 430 wheelsets from passenger vehicles, only 4 could lead to side wear when in the balance position (less than 1%), while of the 2938 wheelsets from freight vehicles, 171 could lead to side wear (almost 6%).As well as the proportion of wheelsets of freight vehicles that contact the gauge side of the rail being much larger than that of passenger vehicles, more freight vehicles use the line (about 3650 freight vehicles and 810 passenger vehicles every day), so the contact points in the side wear area are predicted to result mainly from freight vehicles' wheelsets. Also, note that the average axle load of freight vehicles is about 22 tonnes, larger than the 18 tonne passenger vehicles so the forces transmitted through the contact

points are likely to be larger.

Oil paint was sprayed on the rail surface at Rail:1370, and observations were made of what happened to it after trains passed. When a passenger train passed, there was nearly no marking in the side wear area. However, when a freight train passed, the oil paint in the side wear area was scraped by some wheels.

The wheel/rail contact results agree well with the field test, indicating that the side wear at Rail:1370 is mainly from freight vehicles. Thus, subsequent analyses only use freight vehicles' wheel profiles.

4.2 Side wear from smaller lateral displacements of wheelsets

The NRRD of the 4 passenger vehicle wheelsets that could cause side wear are 1.8, 2.3, 1.4, and 1.1 mm, with corresponding wheelset lateral displacements in balance position of 5.8, 8.2, 5.9, and 1.9 mm respectively.

The NRRD of the 171 freight vehicle wheelsets that could cause side wear are shown in Table 6. The corresponding wheelset lateral displacements in balance position are shown in Fig.10. The proportion of wheelsets that could cause side wear increases with the NRRD. Nearly all wheelsets with a NRRD larger than 4 mm could cause side wear.

Side wear occurs most often when the wheelset lateral displacement is larger than the gauge clearance, but as shown in Fig.10, some wheelsets with small lateral displacements could also cause side wear. For freight vehicles, about 101 wheelsets that could cause side wear have lateral displacements less than 9 mm (the gauge clearance is about 9 mm).

Table 6 NRRD of wheelsets that could cause side wear in freight vehicles

NRRD range/mm	0 - 1	1 - 2	2 - 3	3 - 4	4 - 5	≥ 5
Number of side wear wheelsets	5	25	53	53	20	15
Number of all wheelsets	2344	364	131	62	22	15
Proportion/%	0.2	6.9	40.5	85.5	90.9	100

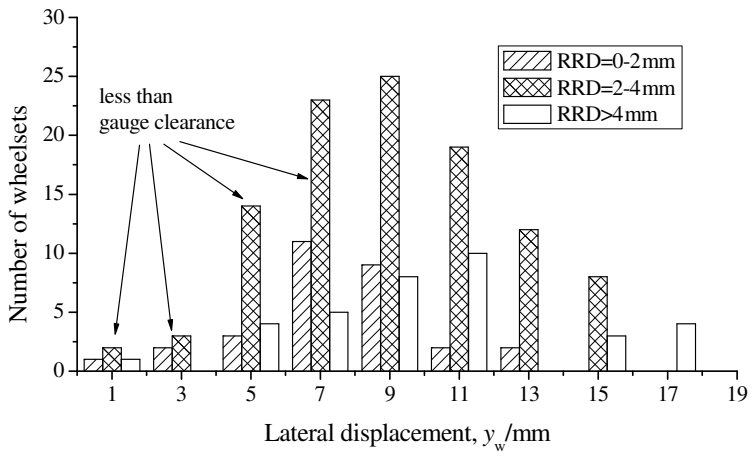

Fig.10. Lateral displacement distributions of wheelsets that could cause side wear in freight vehicles

To investigate how a wheelset with a lateral displacement of less than the gauge clearance in balance position can lead to side wear, a specimen wheelset was examined. The profiles of the wheels on such a wheelset with a y_w of 5.8 mm are shown in Fig.11. It has a NRRD of 2.56 mm. When this wheelset is running on straight track, because the radius of the left wheel is larger than that of the right wheel, the wheelset will move to the right side until it reaches the balance position. In the balance position, the wheelset lateral displacement, and a geometric consideration, predicts that two wheel/rail contact points

will occur on the rail surface, P1 and P2, as shown in Fig.12. One of these is located on the top of the rail and the other, on the rail's gauge corner, could lead to rail side wear. Note that, for any two-point contact, the RRD will not be matched at either contact point, and that a dynamic simulation using this wheelset would predict oscillations about this equilibrium position, so contacts close to both P1 and P2 would be expected.

For the right wheel profile of the above wheelset, hollow wear is 0.55 mm, which causes the wheel's flange root to be closer to the rail than it would be for normal wear. Thus leading to contact with the rail gauge corner being possible with a small lateral displacement of the wheelset.

In order to avoid rail side wear occurring with a small lateral displacement of the wheelset, the rail gauge corner can be ground as shown in Fig.13. The maximum grinding depth Δh_g is measured at the position whose normal makes an angle to the rail centreline of 45°. When Δh_g = 1mm, the RRD function is shown in Fig.14. The wheel/rail contact point in balance position is shown in Fig.15 and, comparing with Fig.11, it is clear that contact P2 no longer occurs.

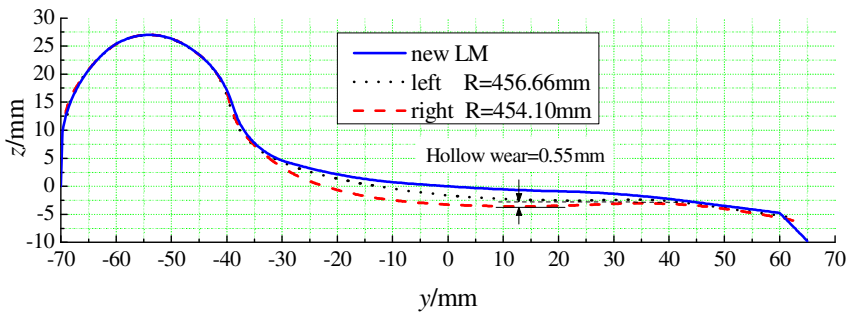

Fig.11.Wheel profiles with NRRD = 2.56 mm

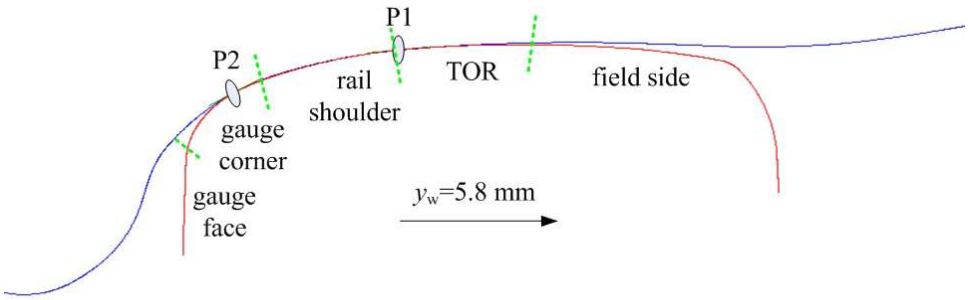

Fig.12. Wheel/rail contact in balance position

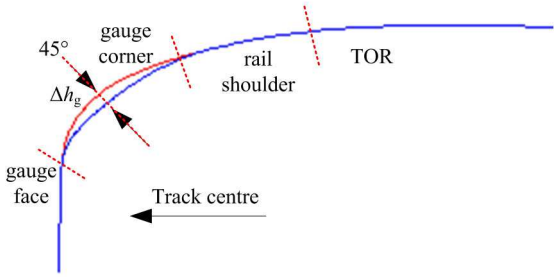

Fig.13. Rail grinding in gauge corner

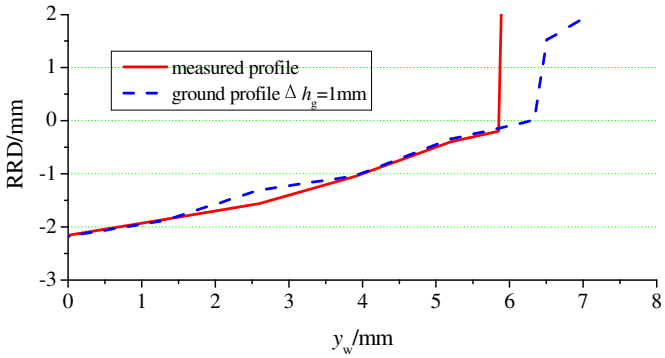

Fig.14. RRD function before and after gauge corner grinding

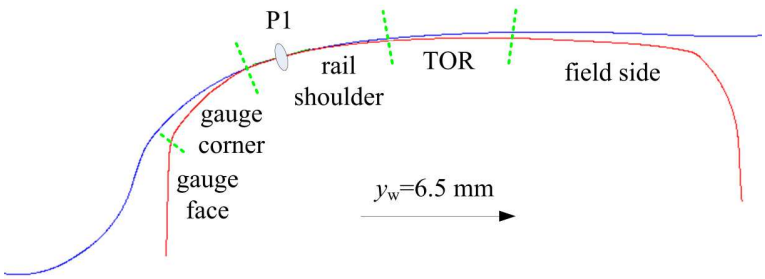

Fig.15. Contact point after gauge corner grinding

Freight vehicles' wheel profiles were used in the static geometric contact calculation to analyse the effect of rail gauge corner grinding. For the two depths, Δh_g = 0.5 mm and Δh_g = 1.0 mm, the distribution of wheel/rail contact points are shown in Fig.16. The radius differences and corresponding lateral displacements of wheelsets that could cause side wear are shown in Table 7 and Fig.17.

When Δh_g = 0.5 mm, 76 wheelsets could cause side wear, while only66 could when Δh_g = 1.0 mm. The effect of rail gauge corner grinding is obvious for the wheelsets for which NRRD ≤ 5 mm, but still some wheelsets with small NRRD could cause side wear.

For those wheelsets that could cause side wear after rail gauge corner grinding, there are only 8 (0.5% of the total) for Δh_g = 0.5 mm and 5 (0.2% of the total) for Δh_g = 1.0 mm with lateral displacements in balance position less than 9mm. This means that rail gauge corner grinding can decrease the proportion of wheelsets that could cause rail side wear.

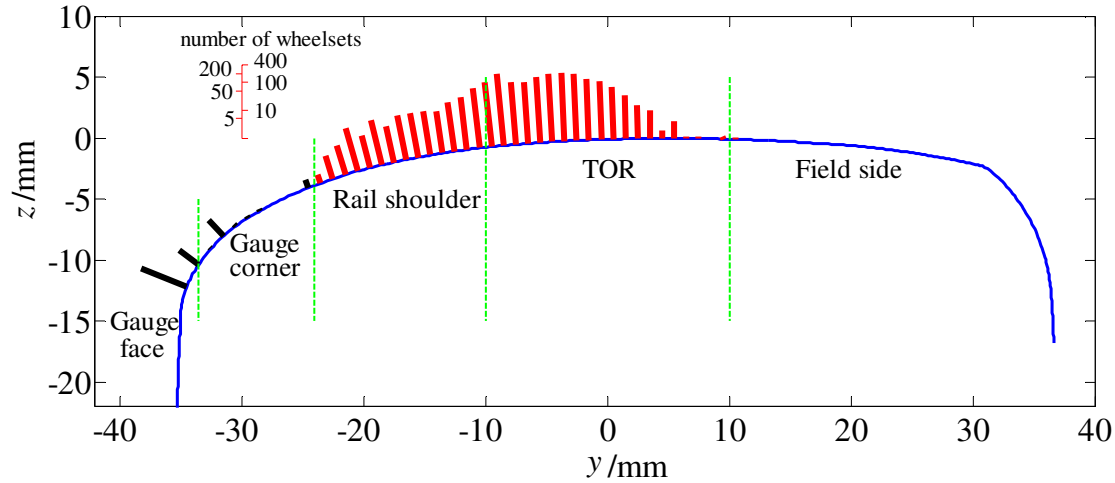

(a) Δh_g = 0.5 mm

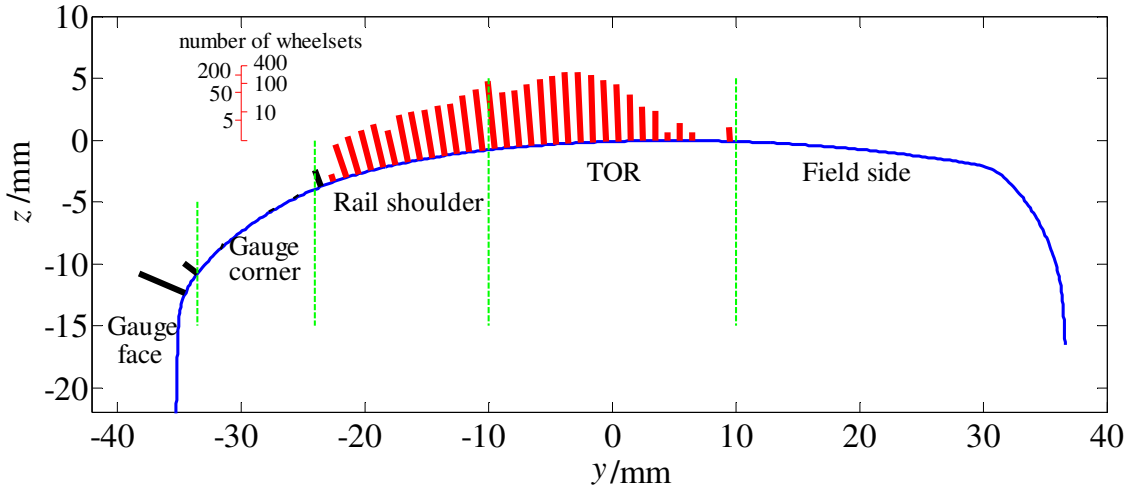

(b) Δh_g = 1.0 mm

Fig.16. Distribution of wheel/rail contact points after gauge corner grinding with a depth of (a) 0.5 mm and (b) 1.0 mm

Table 7: NRRD of wheelsets that could cause side wear after gauge corner grinding

NRRD/mm	0 - 1	1 - 2	2 - 3	3 - 4	4 - 5	≥ 5
Measured profile	5	25	53	53	20	15
Δh_g=0.5mm	2	6	17	26	10	15
Δh_g=1.0 mm	1	4	12	24	10	15

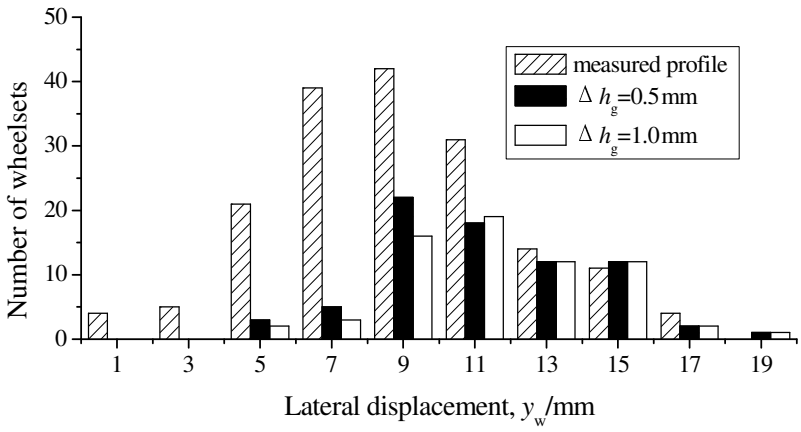

Fig.17. Lateral displacement distributions of wheelsets that could cause side wear for Rail:1370 measured profile, and after gauge corner grinding with a depth of 0.5 and 1.0 mm

4.3 Side wear from low NRRD

Although rail gauge corner grinding can decrease the number of wheelsets that could cause side wear, there are some wheelsets, with NRRDs less than 1mm that could still lead to rail side wear. To investigate this when Δh_g = 1.0 mm, a wheelset with NRRD=1.61mm was selected. Its wheel/rail contact points in balance position are shown in Fig.18. The lateral displacement is 13.0 mm and two-point contact occurs. Although the NRRD is small, the wheelset still exhibits a large lateral displacement and contact on the gauge corner.

Before the wheelset reaches balance position, the contact points are always located on the TOR, sometimes even located on the rail field side. This means that, although the wheelset lateral displacement is larger than the gauge clearance, there is still not enough RRD between the left and right wheel, so the wheelset lateral displacement has to increase, leading to flange contact and the possibility of rail side wear.

Considering the geometry of the wheel and rail profiles, it can be seen that the contact between the wheel flange root and the rail shoulder can produce a larger RRD than that between the TOR and the field side of the rail. If the TOR and rail field side are higher than the rail shoulder, contact cannot occur on the rail shoulder before flange contact. To prevent this, the TOR and rail field side can be ground as shown in Fig.19, where Δh_t is the maximum vertical grinding depth on the rail head.

The RRD function is shown in Fig.20 when Δh_t = 0.5 mm. The resulting contact points when the example wheelset is at balance position are shown in Fig.21.By TOR and field side grinding, because the flange root can contact the rail shoulder rather than TOR, the RRD increases with lateral displacement faster than before. When in the balance position, the wheel/rail contact point is located on the rail shoulder with no flange contact, so there can be no rail side wear.

The distribution of wheel/rail contact points for Δh_t = 0.3 and 0.5 mm are shown in Fig.22. The NRRD of wheelsets that could cause side wear are shown in Table 8.

When Δh_t = 0.3 mm, 72 wheelsets could cause side wear, while 55 could when Δh_t = 0.5 mm. Of the wheelsets that could cause rail side wear, there are none with NRRD smaller than 1 mm. The number with NRRD smaller than 4 mm decreases significantly.

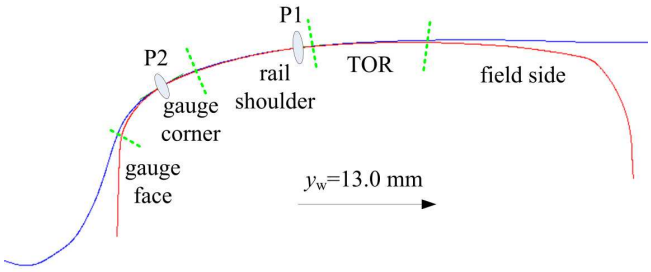

Fig.18. Wheel/rail contact when NRRD=1.61 mm

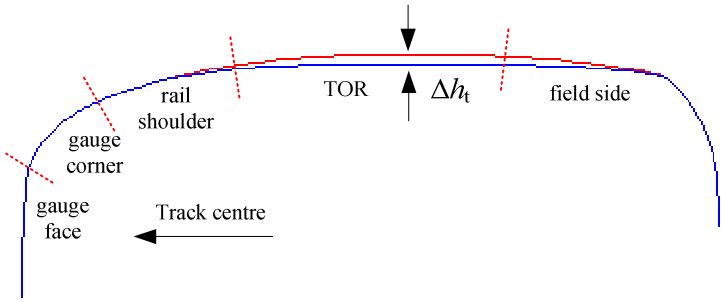

Fig.19. Rail grinding on TOR

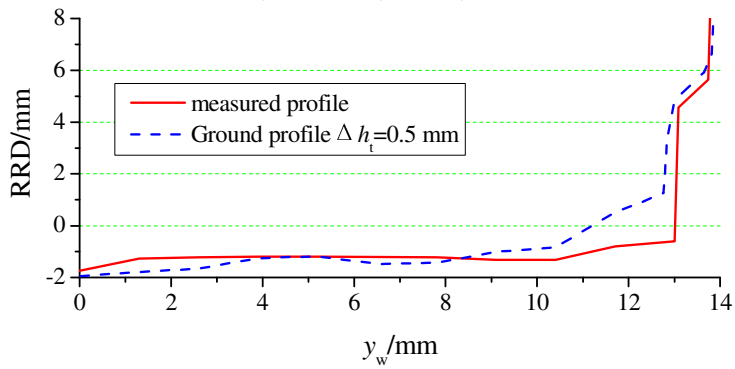

Fig.20. RRD functions after TOR and field side grinding

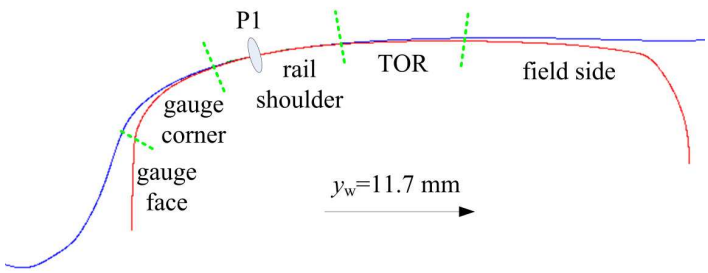

Fig.21. Wheel/rail contact after TOR grinding

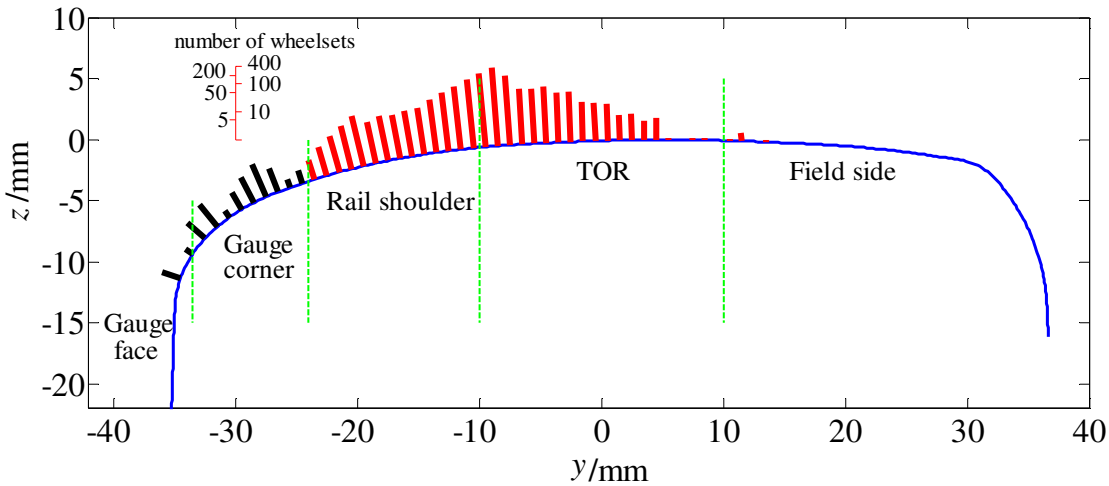

(a) $\Delta h_t = 0.3$ mm

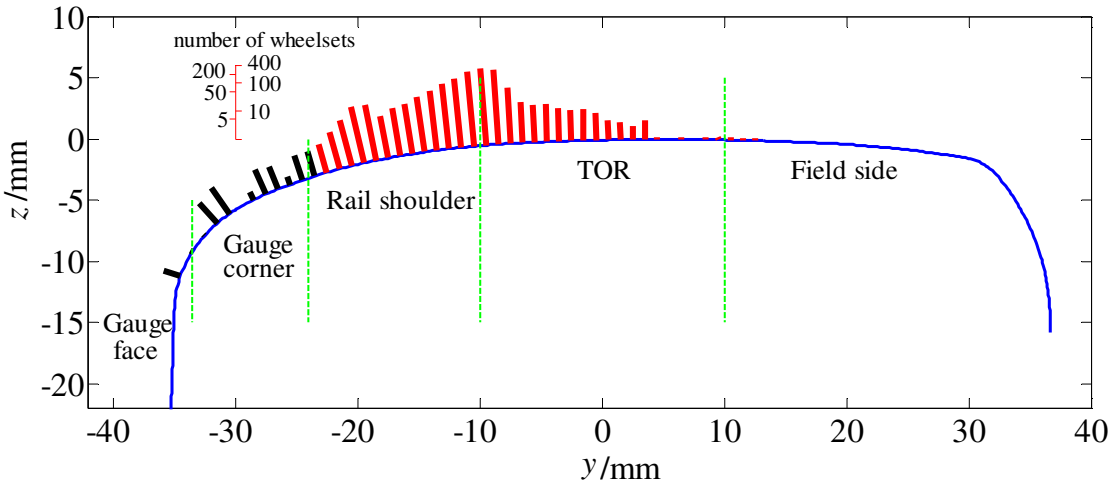

(b) $\Delta h_t = 0.5$ mm

Fig.22. Distribution of wheel/rail contact points after TOR grinding

Table 8 NRRD of side wear wheelsets after TOR grinding

RRD/mm	0 - 1	1 - 2	2 - 3	3 - 4	4 - 5	≥ 5
Measured profile	5	25	53	53	20	15
$\Delta h_t = 0.3$ mm	0	6	11	23	17	15
$\Delta h_t = 0.5$ mm	0	2	4	19	16	14

5. Discussion and rail grinding test

Rail side wear can be associated with wheelsets that have both large and small NRRD. There are two main reasons for rail side wear:

- Wheels with hollow wear and high flange roots can contact the gauge corner with a large NRRD.
- Rails with a top and field side that are much higher than the rail shoulder can cause wheelsets with small NRRD to contact the gauge corner.

Grinding on both the rail gauge corner and the TOR can decrease the number of wheelsets that could cause side wear. Rail gauge corner grinding is effective for wheelsets with hollow wear and high flange root, and rail TOR grinding is effective for wheelsets with smaller NRRD. If the gauge corner and TOR are ground simultaneously, the grinding effect is expected to be better than just grinding the gauge corner or

TOR.

To verify the improvement, Rail:1370 was ground. The rail grinder used in Jing-Hu railway is GMC-96X, which equipped with 96-stone units. For each stone unit, the rated motor power is 22 kW, and the diameter of grinding stone is 254 mm.

Before the grinding work, the 96-stone units were arranged with different angles according to the differences between the measured rail profile and the aim profile. The working speed of the rail grinder is about 12-18 km/h and the surface rotating speed of grinding wheel and rail steel is about 3600 rpm.

The rail profile after grinding is shown in Fig.23. Material was mainly removed from the gauge corner, TOR, and field side; the rail shoulder was not ground. The maximum grinding depth on the gauge corner was 0.5mm, and the maximum grinding depth on the TOR was 0.9mm.

The distribution of wheel/rail contact points on the ground rail profile is shown in Fig.24. For the passenger vehicles, no wheelsets contact the gauge corner or gauge face. For freight vehicles, 27 wheelsets could lead to side wear after grinding. All the contact points for these wheelsets occur at the rail gauge face, but all the NRRDs of these wheelsets are larger than 4mm. For the wheelsets with larger NRRD, rail grinding cannot avoid side wear completely, so larger NRRD wheelsets should be controlled by the vehicle operators.

For freight vehicles, there are a few wheel/rail contact points on the field side of the rail. The main reason is that the grinding depth on the field side is less than that on the TOR.

A month after rail grinding, the rail surface is shown in Fig.25. It can be seen that almost all the contact area is on the TOR and rail shoulder, and the rail gauge face and field side have only minimal contact. The rail surface agrees well with the calculation results shown in Fig.24.

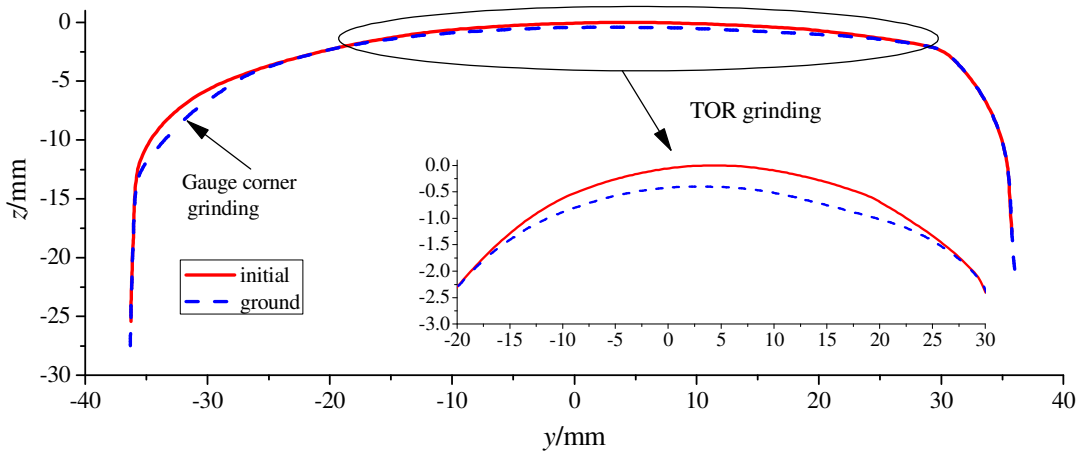

Fig.23. Ground rail profile at 1370 km position

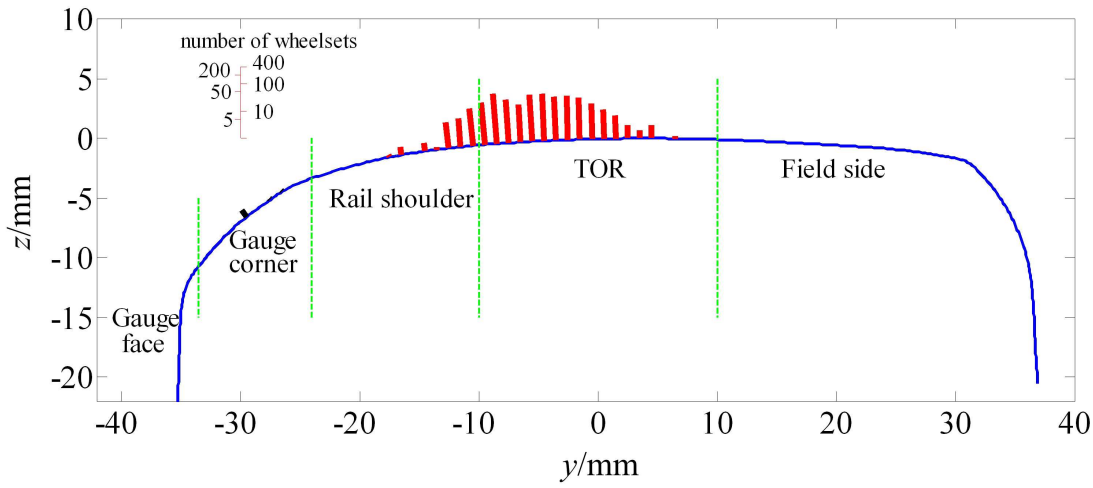

(a) Passenger vehicle

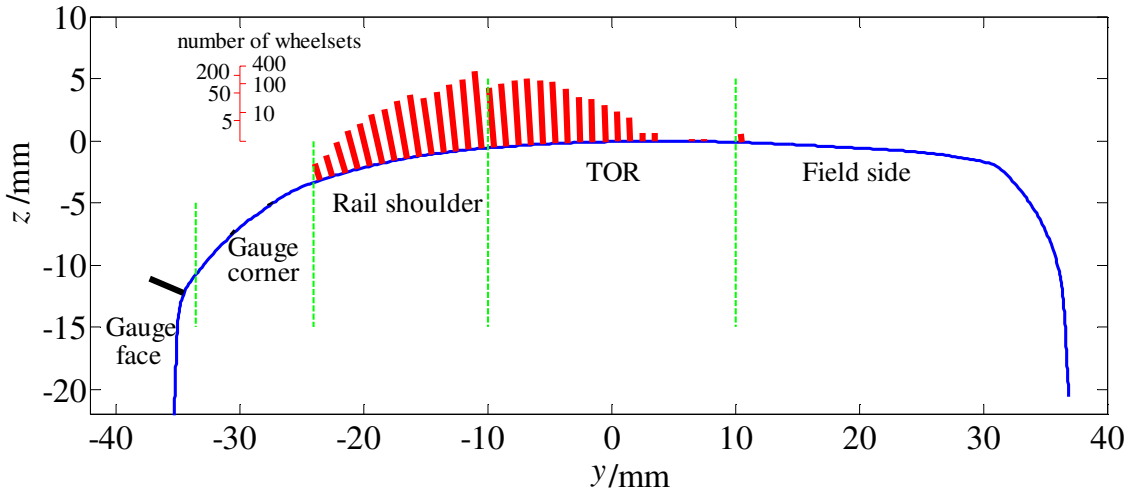

(b) Freight vehicle

Fig.24. Distribution of wheel/rail contact points after rail grinding

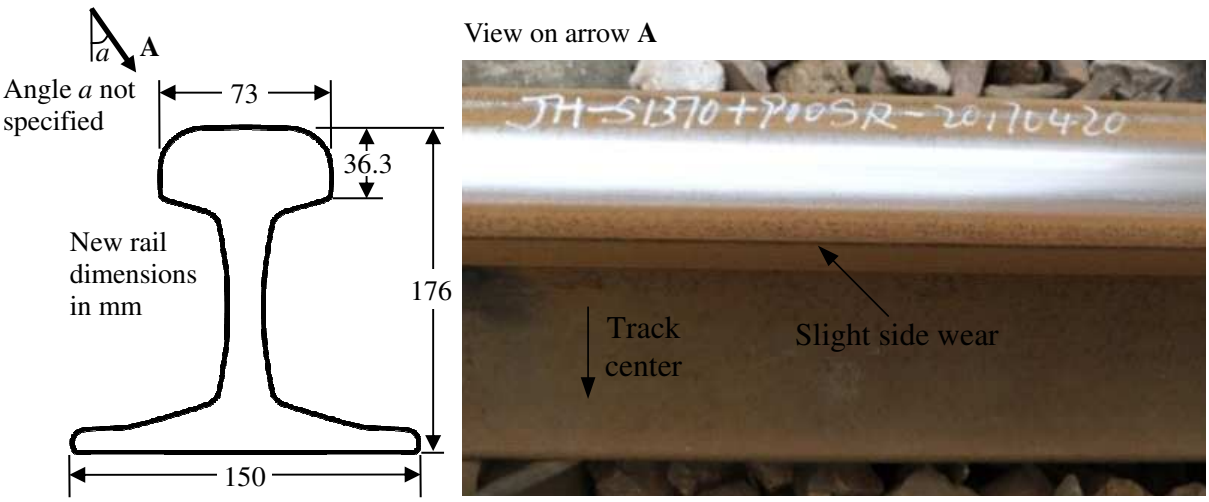

Fig.25. Rail surface after rail grinding

6. Conclusions

Dynamic models of passenger and freight vehicles were built to analyse the dynamic behaviour at the 1370 km position on the Jing-Hu railway in China. A range of both passenger and freight vehicles were shown to be stable despite the wheelsets having different NRRD, supporting site observations that side wear in this straight track was not caused by hunting.

On straight track, wheelsets will move to a balance position that depends on the NRRD, with some wheel/rail contact points located on the rail gauge corner and gauge face; wear at these locations is defined to be side wear. Lower wheelset lateral displacements could lead to side wear if the rail has a higher gauge corner. If the TOR and rail field sides are too high, contact cannot occur on the rail shoulder before flange contact, so wheelsets could cause rail side wear with lower NRRD.

Rail gauge corner grinding or TOR grinding can decrease the number of wheelsets that could cause side wear. It is predicted to be more effective when the rail gauge corner and TOR are both ground at the same time. The rail profile at the 1370-km position on the Jing-Hu railway was ground like this, and the resulting indications on the rail surface agree well with the calculation results. It is still possible for there to be side wear from wheelsets with larger NRRD. Such wheelsets should be controlled and replaced by the vehicle's operator.

Due to the large number of wheel profiles, this paper used static wheel/rail geometry contacts instead of dynamic calculations to assess the causes of rail side wear in straight track. Although the findings in the paper have not been verified by dynamic simulation, the track results demonstrate the applicability of the method. Since its calculation speed is so fast, this method can be used to consider actual wheel/rail contact conditions.

Acknowledgements

This work was supported by the National Natural Science Foundation of China (51305359), the Fundamental Research Funds for the Central Universities（2682016CX029）and the Young Scientific Innovation Team of Science and Technology of Sichuan (2017TD0017).

References

[1] G. Evans, Managing rail profile, Ironmaking & Steelmaking 40 (2013) 115-119.

[2] E. Magel, J. Kalousek, The application of contact mechanics to rail profile design and rail grinding, Wear 253 (2002) 308-316.

[3] E. Magel, J. Kalousek, Designing and assessing wheel/rail profiles for improved rolling contact fatigue and wear performance, J. Rail Rapid Transit 231(2017) 805-818.

[4] H. Y. Choi, D.H. Lee, C. Song, J. Lee, Optimization of rail profile to reduce wear on curved track, International Journal of Precision Engineering and Manufacturing 14 (2013) 619-625.

[5] I. Y. Shevtsov, V. L. Markine, C. Esveld, Design of railway wheel profile taking into account rolling contact fatigue and wear, Wear265(2008) 1273-1282.

[6] W. M. Zhai, J. M. Gao, P F Liu. Reducing rail side wear on heavy-haul railway curves based on wheel–rail dynamic interaction, Veh. Syst. Dyn. 52 (2014) 440-454.

[7] F. Braghin, R. Lewis, R. S. Dwyer, A mathematical model to predict railway wheel profile evolution due to wear, Wear261(2006) 1253–1264.

[8] R. Enblom, M. Berg. Simulation of railway wheel profile development due to wear, Wear 258(2005) 1055–1063.

[9] R. Lewis, U. Olofsson, Mapping rail wear regimes and transitions, Wear 257 (2004) 721-729.

[10] M. Ignesti, A. Innocenti, L. Marini, E. Meli, A. Rindi. Development of a model for the simultaneous analysis of wheel

and rail wear in railway systems, Multibody System Dynamics 31 (2014) 191-240.

[11] A. Innocenti, L. Marini, E. Meli, G. Pallini, A. Rindi, Development of a wear model for the analysis of complex railway networks, Wear 309 (2014) 174-191

[12] T. G. Pearce, N. D. Sherratt, Prediction of wheel profile wear, Wear 144(1991) 343–351.

[13] I. Zobory, Prediction of wheel/rail profile wear, Veh.Syst.Dyn. 28, (1997) 221–259.

[14] T. Jendel, Prediction of wheel profile wear-comparisons with filed measurements, Wear 253 (2002) 89–99.

[15] X.S. Jin, Z..F. Wen, X.B. Xiao, A numerical method for prediction of curved rail wear, Multibody System Dynamics 18 (2007) 531-557.

[16] X. Li, X.S. Jin, Z.F. Wen, A new integrated model to predict wheel profile evolution due to wear, Wear 271 (2011) 227-237.

[17] M. Adachi, A. Matsumoto, Improvement of curving performance by expansion of gauge widening and additional measures, J. Rail Rapid Transit 226 (2012) 203-215.

[18] I. Povilaitiene, I. Z. Kamaitis, I. Podagelis, Influence of gauge width on rail side wear on track curves, Journal of Civil Engineering and Management, 12 (2006) 255-260.

[19] Y.J. Ji, L.H. Ren, J. Wang, Mechanism and affecting factors of Translohr tramway guide rail side wear, Proceedings of the Institution of Mechanical Engineers, Part C: Journal of Mechanical Engineering Science 231(2017) 3898-3912.

[20] D.B. Cui, W.H. Zhang, G.D. Tian, Designing the key parameters of EMU bogie to reduce side wear of rail, Wear 366-367 (2016) 49–59.

[21] S. Descartes, A. Saulot, C. Godeau, S. Bondeux, C. Dayot, Y. Berthier, Wheel flange/rail gauge corner contact lubrication: Tribological investigations, Wear 271 (2011) 54-61.

[22] M. G. Uddin, G. Chattopadhyay, M. Rasul, Development of effective performance measures for wayside rail curve lubrication in heavy haul lines, J. Rail Rapid Transit 228(2014) 481-495.

[23] S. A. Khan, I. Persson, J. Lundberg, C. Stenström, Prediction of top-of-rail friction control effects on rail RCF suppressed by wear, Wear 15 (2017) 106-114.

[24] X. Lu, T. W. Makowsky, D.T. Eadie, K. Oldknow, J. L. Xue, J. Z. Jia, G. B. Li, X. H. Meng, Y. D. Xu, Y. Zhou, Friction management on a Chinese heavy haul coal line, J. Rail Rapid Transit 226 (2012) 630-640.

[25] Y. Satoh, K. Iwafuchi, Effect of rail grinding on rolling contact fatigue in railway rail used in conventional line in Japan, Wear 265 (2008) 1342–1348.

[26] K. Sawley, C. Urban,R. Walker, The effect of hollow-worn wheels on vehicle stability in straight track, Wear 258 (2005) 1100-1108.

[27] P. Wang, X. C. Ma, J. Wang, J. M. Xu, R. Chen, Optimization of rail profiles to improve vehicle running stability in switch panel of high-speed railway turnouts, Mathematical Problems in Engineering, 2017..[Online]

[28] SIMPACK. Available at http://www.simpack.com.

[29] J.J. Kalker, A fast algorithm for the simplified theory of rolling contact, Veh. Syst. Dyn.11(1982)1–13.